CrossMark

J. Fluid Mech. (2016), *vol.* 803, *pp.* 94–118. © Cambridge University Press 2016
doi:10.1017/jfm.2016.507

Oscillatory Marangoni flows with inertia

Orest Shardt[1,†], Hassan Masoud[1,2] and Howard A. Stone[1]

[1]Department of Mechanical and Aerospace Engineering, Princeton University, Princeton, NJ 08544, USA

[2]Department of Mechanical Engineering, University of Nevada, Reno, NV 89557, USA

(Received 5 April 2016; revised 1 July 2016; accepted 26 July 2016;
first published online 19 August 2016)

When the surface of a liquid has a non-uniform distribution of a surfactant that lowers surface tension, the resulting variation in surface tension drives a flow that spreads the surfactant towards a uniform distribution. We study the spreading dynamics of an insoluble and non-diffusing surfactant on an initially motionless liquid. We derive solutions for the evolution over time of sinusoidal variations in surfactant concentration with a small initial amplitude relative to the average concentration. In this limit, the coupled flow and surfactant transport equations are linear. In contrast to exponential decay when the inertia of the flow is negligible, the solution for unsteady Stokes flow exhibits oscillations when inertia is sufficient to spread the surfactant beyond a uniform distribution. This oscillatory behaviour exhibits two properties that distinguish it from that of a simple harmonic oscillator: the amplitude changes sign at most three times, and the decay at late times follows a power law with an exponent of $-3/2$. As the surface oscillates, the structure of the subsurface flow alternates between one and two rows of counter-rotating vortices, starting with one row and ending with two during the late-time monotonic decay. We also examine numerically the evolution of the surfactant distribution when the system is nonlinear due to a large initial amplitude.

Key words: interfacial flows (free surface), low-Reynolds-number flows

1. Introduction

Systems with flow coupled to heat transfer, mass transfer or reactions can exhibit oscillations when spatial variations in temperature or composition create non-uniform surface tensions. Examples of such oscillatory systems include the periodic ejection of fine droplets from a pendant water drop in oil (Fernandez & Homsy 2004), the beating of an oil lens on water (Stocker & Bush 2007) and the intermittent flow of a free water surface due to diffusion of an organic molecule from a droplet below the surface (Kovalchuk *et al.* 1999). The time scales of the oscillations range from several tenths of a second in the first two examples to minutes in the third example. In all of these systems, the flows are driven by spatial variations in the concentration of surface active molecules (surfactants), and therefore also surface tension, along a surface. In general, flows driven by spatially varying surface tension are referred to as Marangoni flows, and they occur in many natural phenomena and industrial processes

†Email address for correspondence: oshardt@princeton.edu

https://doi.org/10.1017/jfm.2016.507 Published online by Cambridge University Press

(Scriven & Sternling 1960). In this paper, we study the spreading of surfactants on a free surface and find that oscillations also occur in this simpler system.

When surfactants are deposited on the free surface of a liquid, they typically locally reduce the surface tension, driving a flow that spreads the surfactant over the surface. The spreading of surfactants used to treat surfactant deficiency in the lungs of prematurely born infants (Grotberg 1994) motivated early studies of spreading on thin films (Jensen & Grotberg 1992; Jensen 1994). Such spreading flows on thin films can develop fingering instabilities (Troian, Herbolzheimer & Safran 1990; Matar & Troian 1999; Edmonstone, Craster & Matar 2006; Jensen & Naire 2006). In addition, surfactant spreading on deep fluid layers has been studied (Jensen 1995; Thess 1996; Dussaud & Troian 1998).

Interest in Marangoni flows has also been driven by their role in the motion of particles (Pimienta & Antoine 2014) and organisms (Bush & Hu 2006) along interfaces. A classic example of particle motion is the erratic movement of camphor when it is placed on water (Rayleigh 1890; Nakata *et al.* 1997; Nakata & Hayashima 1998). This motion occurs due to gradients in surface tension around the particles that are created by non-uniform spreading of camphor molecules, which act as a surfactant. These systems are interesting from a thermodynamic perspective because chemical energy is converted to kinetic energy in the absence of a temperature gradient (Nakata *et al.* 1997). Such isothermal conversion of chemical to kinetic energy also occurs in biological locomotion, in contrast to the large temperature differences required by heat engines. In fact, some organisms directly exploit Marangoni flows for propulsion (Bush & Hu 2006). For example, the water-walking insects Microvelia can reach speeds of 17 cm s^{-1}, which is twice their walking speed, by releasing a surfactant.

In addition to driving the motion of individual particles at interfaces, spatial variations in surfactant concentration and surface tension are responsible for coupling the motion of several particles (Kohira *et al.* 2001; Nakata, Doi & Kitahata 2005). For individual particles, the speeds of disks (Lauga & Davis 2012) and spheroids (Masoud & Stone 2014) that asymmetrically release insoluble surfactants have been determined. The collective motion of particles on an interface that locally increase surface tension by reacting with a surface active compound in the adjacent fluid layer has also been studied. Such particles aggregate due to the higher tension in regions of the surface with a higher particle concentration. The possibility of a collapse of particle distributions to points in finite time has been demonstrated (Masoud & Shelley 2014), but the effects of inertia were not considered.

Here, we consider the spreading of an insoluble surfactant, which reduces surface tension, on a deep layer of Newtonian fluid that is initially motionless. For unsteady Stokes flow (the appropriate linearized version of the Navier–Stokes equations) with sufficient inertia (i.e. an appropriately defined Reynolds number exceeds a critical value), we find that sinusoidal spatial variations in surfactant concentration oscillate as they decay in time to a uniform distribution. Such longitudinal surface oscillations are distinct from longitudinal waves due to surface elasticity (Lucassen 1968*a*,*b*) and interfacial instability during transfer of a soluble surfactant across an interface (Sternling & Scriven 1959; Velarde & Chu 1989). In § 2, we present the coupled initial value problem for surfactant spreading and flow. We derive, in § 3, solutions to this problem for the limit of small-amplitude variations in surfactant concentration and negligible surfactant diffusion. In this limit, the flow and surfactant transport equations are linear, and solutions are provided for both the limits of quasi-steady Stokes flow and unsteady Stokes flow of the fluid. Nonlinear surfactant spreading and fluid flow due to initial concentration variations with finite amplitude are studied numerically in § 4 and compared with the behaviour in the linear limit.

https://doi.org/10.1017/jfm.2016.507 Published online by Cambridge University Press

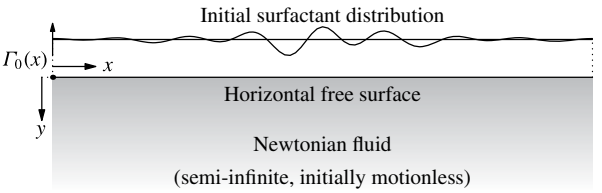


FIGURE 1. Schematic of the modelled system. An arbitrary initial distribution of insoluble surfactant $\Gamma_0(x)$ drives the incompressible flow of a semi-infinite layer of Newtonian fluid, which redistributes the surfactant.

2. Problem definition

Consider the transport of an insoluble surfactant along the free surface of a semi-infinite fluid domain in two dimensions, as illustrated in figure 1. Let the x axis be parallel to the fluid surface, which is assumed to remain flat, and y be perpendicular to it and extend into the fluid. The surface is therefore located at $y = 0$, and fluid is present in the half-plane $y \in [0, \infty)$. The surface concentration of the surfactant $\Gamma(x, t)$ evolves according to the advection–diffusion equation

$$\frac{\partial \Gamma}{\partial t} + \frac{\partial}{\partial x}(\Gamma u_s) = D_s \frac{\partial^2 \Gamma}{\partial x^2}, \tag{2.1}$$

where u_s is the x component of the fluid velocity $\boldsymbol{u} = (u, v)$ at $y = 0$ and D_s is the diffusivity of the surfactant along the surface. The surfactant concentration determines the surface tension γ through the linear equation of state

$$\gamma = \gamma_0 - \alpha \Gamma, \tag{2.2}$$

where γ_0 is the tension of a surfactant-free surface and α is the proportionality constant. This simplification is common and used widely in the literature. It follows that the mean surface tension $\bar{\gamma}$ on a surface is $\gamma_0 - \alpha \bar{\Gamma}$, where $\bar{\Gamma}$ is the mean surfactant concentration. We restrict our attention to the case of a surfactant that reduces surface tension, i.e. $\alpha > 0$. We assume that the bulk fluid is Newtonian with dynamic viscosity μ and density ρ, and the flow is incompressible. The fluid velocity $\boldsymbol{u}(x, y, t)$ and pressure $p(x, y, t)$ therefore evolve according to

$$\rho \left(\frac{\partial \boldsymbol{u}}{\partial t} + \boldsymbol{u} \cdot \nabla \boldsymbol{u} \right) = -\nabla p + \mu \nabla^2 \boldsymbol{u} \tag{2.3}$$

together with the continuity equation

$$\nabla \cdot \boldsymbol{u} = 0. \tag{2.4}$$

Variations in surface tension along the surface of the fluid (at $y = 0$) impose a Marangoni stress on it, which leads to the boundary condition

$$\left. \frac{\partial u}{\partial y} \right|_{y=0} = -\frac{1}{\mu} \frac{\partial \gamma}{\partial x} = \frac{\alpha}{\mu} \frac{\partial \Gamma}{\partial x}. \tag{2.5}$$

https://doi.org/10.1017/jfm.2016.507 Published online by Cambridge University Press

We consider the initial value problem of a given surfactant distribution on an initially motionless fluid and determine how the surfactant distribution and flow evolve over time. This problem has the initial conditions

$$\Gamma(x, 0) = \Gamma_0(x), \quad \boldsymbol{u}(x, y, 0) = \boldsymbol{0} \tag{2.6a,b}$$

and the boundary conditions are (2.5) together with

$$v(x, 0, t) = 0, \quad |\boldsymbol{u}| = 0 \quad \text{as } y \to \infty, \quad p = 0 \quad \text{as } y \to \infty, \tag{2.7a–c}$$

for $t > 0$. The ambient constant pressure is a reference that is set equal to zero. The first boundary condition arises from the assumption of a flat interface. While the normal component of the velocity is zero along the surface, the tangential component varies due to the non-uniform surfactant concentration and stress.

We now non-dimensionalize the governing equations, using the idea that there is a Marangoni flow driven by small deviations in the surfactant concentration about a mean value. We start with the Marangoni surface stress, equation (2.5), that provides the characteristic speed of the system. We proceed by introducing $\tilde{x} = x/\lambda$, $\tilde{y} = y/\lambda$, $\tilde{u} = u/\varepsilon u^*$, and $\tilde{\Gamma} = (\Gamma - \bar{\Gamma})/(\varepsilon\bar{\Gamma})$, where the length scale λ, mean surfactant concentration $\bar{\Gamma}$ and amplitude of the variation in surfactant concentration $\varepsilon\bar{\Gamma}$ are all properties of the initial surfactant distribution. Choosing $u^* = \alpha\bar{\Gamma}/\mu$, we are left with

$$\left.\frac{\partial\tilde{u}}{\partial\tilde{y}}\right|_{\tilde{y}=0} = \frac{\partial\tilde{\Gamma}}{\partial\tilde{x}}. \tag{2.8}$$

Recalling the relationship between the surface tension and surfactant concentration, equation (2.2), we see that $\varepsilon\alpha\bar{\Gamma}$ is the amplitude of the variation in surface tension. Therefore, εu^* can be interpreted as a Marangoni speed, the ratio of the surface tension difference that drives flow and the resisting viscous stress.

Next, the surfactant advection–diffusion equation (2.1) becomes

$$\frac{\partial\tilde{\Gamma}}{\partial\tilde{t}} + \varepsilon\frac{\partial}{\partial\tilde{x}}(\tilde{\Gamma}\tilde{u}_s) + \frac{\partial\tilde{u}_s}{\partial\tilde{x}} = Pe_s^{-1}\frac{\partial^2\tilde{\Gamma}}{\partial\tilde{x}^2}, \tag{2.9}$$

where $\tilde{u}_s = u_s/(\varepsilon u^*)$, $\tilde{t} = t/t^*$, and $t^* = \lambda/u^*$ is an advective time scale. The Péclet number $Pe_s = u^*\lambda/D_s$ is the ratio of the diffusive time scale λ^2/D_s and the advective time scale λ/u^*. Using this scaling together with $\tilde{p} = p\lambda/(\varepsilon\mu u^*)$, the Navier–Stokes and continuity equations become

$$Re\left(\frac{\partial\tilde{\boldsymbol{u}}}{\partial\tilde{t}} + \varepsilon\tilde{\boldsymbol{u}}\cdot\tilde{\boldsymbol{\nabla}}\tilde{\boldsymbol{u}}\right) = -\tilde{\boldsymbol{\nabla}}\tilde{p} + \tilde{\nabla}^2\tilde{\boldsymbol{u}} \tag{2.10}$$

and

$$\tilde{\boldsymbol{\nabla}}\cdot\tilde{\boldsymbol{u}} = 0, \tag{2.11}$$

where $\tilde{\boldsymbol{u}} = \boldsymbol{u}/(\varepsilon u^*)$. The Reynolds number is defined according to $Re = \rho u^*\lambda/\mu = \rho\alpha\bar{\Gamma}\lambda/\mu^2 = \rho(\gamma_0 - \bar{\gamma})\lambda/\mu^2$.

In non-dimensional form, we seek the solution to equations (2.9), (2.10) and (2.11) with the initial conditions

$$\tilde{\Gamma}(\tilde{x}, 0) = \tilde{\Gamma}_0(\tilde{x}), \quad \tilde{\boldsymbol{u}}(\tilde{x}, \tilde{y}, 0) = \boldsymbol{0} \tag{2.12a,b}$$

and the boundary conditions

$$\tilde{v}(\tilde{x}, 0, \tilde{t}) = 0, \quad \left.\frac{\partial\tilde{u}}{\partial\tilde{y}}\right|_{\tilde{y}=0} = \frac{\partial\tilde{\Gamma}}{\partial\tilde{x}}, \quad |\tilde{\boldsymbol{u}}| = 0 \quad \text{as } \tilde{y} \to \infty, \quad \text{and} \quad \tilde{p} = 0 \quad \text{as } \tilde{y} \to \infty. \tag{2.13a–d}$$

https://doi.org/10.1017/jfm.2016.507 Published online by Cambridge University Press

3. Analytical solutions

In the limit of low Pe_s, we expect smoothing of the surfactant distribution due to diffusion without significant motion of the underlying fluid. The case of high Pe_s is more interesting and relevant to physical systems, and we now pursue analytical solutions for the limit $Pe_s \to \infty$. We further consider the limit of small variations in surfactant concentration relative to the average concentration, i.e. $\varepsilon \to 0$. This limit has two effects on the governing equations: the nonlinear terms vanish in both the surfactant and flow equations, (2.9) and (2.10) respectively, leaving the linear system

$$\frac{\partial \tilde{\Gamma}}{\partial \tilde{t}} + \frac{\partial \tilde{u}_s}{\partial \tilde{x}} = 0, \tag{3.1a}$$

$$Re \frac{\partial \tilde{\boldsymbol{u}}}{\partial \tilde{t}} = -\tilde{\boldsymbol{\nabla}} \tilde{p} + \tilde{\nabla}^2 \tilde{\boldsymbol{u}}, \tag{3.1b}$$

$$\tilde{\boldsymbol{\nabla}} \cdot \tilde{\boldsymbol{u}} = 0. \tag{3.1c}$$

The boundary conditions remain unchanged. In studies of thermocapillary motion of drops, the nonlinear convective term in the transport equation for the temperature in the continuous phase is similarly negligible compared to the transient term (Lavrenteva & Nir 2001). Here, however, the surface dilation term must be included in the surfactant dynamics (3.1*a*) (due to non-zero $\partial \tilde{u}_s / \partial \tilde{x}$ along the surface), and changes in surfactant concentration therefore occur due to expansion or contraction of the surface.

We now proceed to find the solution for this linear initial value problem, first making no assumptions about the form of the initial surfactant distribution, i.e. letting $\tilde{\Gamma}_0(\tilde{x})$ be arbitrary. Additional details about the derivation are provided in appendix A. Since we make frequent use of Fourier ($\mathscr{F}$) transforms with respect to $\tilde{x}$, Laplace ($\mathscr{L}$) transforms with respect to $\tilde{t}$, and their inverses, we use the notation

$$\hat{p}(k, \tilde{y}, \tilde{t}) = \mathscr{F}\{p(\tilde{x}, \tilde{y}, \tilde{t})\} \iff p(\tilde{x}, \tilde{y}, \tilde{t}) = \mathscr{F}^{-1}\{\hat{p}(k, \tilde{y}, \tilde{t})\}, \tag{3.2}$$

$$\check{p}(k, \tilde{y}, s) = \mathscr{L}\{\hat{p}(k, \tilde{y}, \tilde{t})\} \iff \hat{p}(k, \tilde{y}, \tilde{t}) = \mathscr{L}^{-1}\{\check{p}(k, \tilde{y}, s)\} \tag{3.3}$$

for the transformations and the transformed variables, shown here for the pressure. In the transformed functions, k is the wavenumber and s is the complex frequency. We take the divergence of (3.1*b*) and a Fourier transform in $\tilde{x}$ to obtain

$$-k^2 \hat{p} + \frac{\partial^2 \hat{p}}{\partial \tilde{y}^2} = 0. \tag{3.4}$$

Ensuring boundedness as $\tilde{y} \to \infty$, the solution for the pressure is

$$\hat{p}(k, \tilde{y}, \tilde{t}) = \hat{p}_0(k, \tilde{t}) \exp(-|k|\tilde{y}), \quad \check{p}(k, \tilde{y}, s) = \check{p}_0(k, s) \exp(-|k|\tilde{y}), \tag{3.5a,b}$$

where $\hat{p}_0(k, \tilde{t})$ is the pressure at the surface and remains to be determined. Now, taking the Fourier and Laplace transforms of the $\tilde{y}$ component of the momentum equation (3.1*b*) yields

$$(Re\, s + k^2)\check{v} - \frac{\partial^2 \check{v}}{\partial \tilde{y}^2} = |k|\, \check{p}_0(k, s) \exp(-|k|\tilde{y}). \tag{3.6}$$

https://doi.org/10.1017/jfm.2016.507 Published online by Cambridge University Press

Retaining the terms that are bounded as $\tilde{y} \to \infty$ and using $\breve{v} = 0$ at $\tilde{y} = 0$, the solution is

$$\breve{v}(k, \tilde{y}, s) = \frac{|k|\,\breve{p}_0(k, s)}{Re\, s}\left[\exp(-|k|\tilde{y}) - \exp\left(-\tilde{y}\sqrt{k^2 + Re\, s}\right)\right]. \tag{3.7}$$

From the incompressibility constraint $ik\breve{u} + \partial\breve{v}/\partial\tilde{y} = 0$ we find that

$$\breve{u}(k, \tilde{y}, s) = \frac{ik\,\breve{p}_0(k, s)}{|k| Re\, s}\left[\sqrt{k^2 + Re\, s}\exp\left(-\tilde{y}\sqrt{k^2 + Re\, s}\right) - |k|\exp(-|k|\tilde{y})\right]. \tag{3.8}$$

At the surface ($\tilde{y} = 0$), the solutions simplify to

$$\breve{u}(k, 0, s) = \frac{ik}{|k|}\breve{p}_0(k, s)\frac{\sqrt{k^2 + Re\, s} - |k|}{Re\, s}, \tag{3.9a}$$

$$\breve{v}(k, 0, s) = 0, \tag{3.9b}$$

$$\breve{p}(k, 0, s) = \breve{p}_0(k, s). \tag{3.9c}$$

The surface stress boundary condition, equation (2.8), couples the flow and surfactant evolution. Taking its Fourier and Laplace transforms, we obtain

$$\breve{p}_0(k, s) = -|k|\,\breve{\Gamma}(k, s). \tag{3.10}$$

3.1. *Solution for a single mode*

To this point, the derivation has considered an arbitrary initial surfactant distribution $\tilde{\Gamma}_0(\tilde{x})$, and we now restrict our attention to a particular distribution: a single sinusoidal mode. Though a pure sinusoid is an unlikely initial condition for a physical system, the solution for any periodic initial condition can be expressed as a series of the solutions for individual modes due to the linearity of the governing system of equations. Furthermore, the solution for a pure sinusoid is useful because the fundamental mode decays slowest, as we will show, and therefore determines the late-time dynamics. Choosing the length scale λ to be the wavelength of the initial sinusoidal variation in the surfactant concentration, the initial distribution $\tilde{\Gamma}_0(\tilde{x})$ is

$$\tilde{\Gamma}_0(\tilde{x}) = \sin(2\pi\tilde{x}). \tag{3.11}$$

We now take the Fourier and Laplace transforms of the surfactant evolution equation (3.1*a*) to obtain

$$s\breve{\Gamma}(k, s) - \hat{\Gamma}_0(k) + ik\breve{u}_s(k, s) = 0, \tag{3.12}$$

where $\breve{u}_s(k, s) = \breve{u}(k, 0, s)$ and $\hat{\Gamma}_0(k) = \hat{\Gamma}(k, 0)$. Substituting (3.9*a*) and (3.10), we arrive at the Laplace-domain solution for the surfactant evolution:

$$\breve{\Gamma}(k, s) = \frac{1}{s + \dfrac{|k|^3}{Re\, s}\left(\sqrt{1 + \dfrac{Re\, s}{k^2}} - 1\right)}\hat{\Gamma}_0(k). \tag{3.13}$$

For the initial condition we are interested in, a single sinusoidal mode, we have $\hat{\Gamma}_0(k) = -i\pi\,\mathrm{sgn}(k)\,\delta(|k| - 2\pi)$, where $\delta(\cdot)$ is the Dirac delta function and $\mathrm{sgn}(\cdot)$ is

https://doi.org/10.1017/jfm.2016.507 Published online by Cambridge University Press

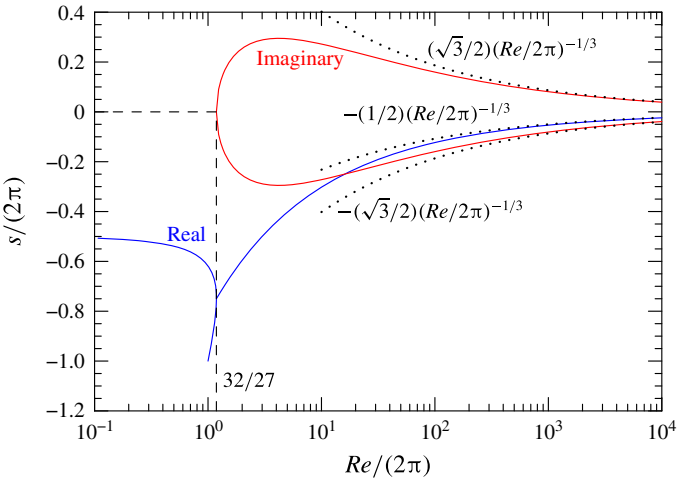


FIGURE 2. (Colour online) Poles of the Laplace-domain solution for the surfactant evolution (3.14). The blue curve shows the real part of the poles, and the red curve shows their imaginary part. The dotted lines show the components of the poles in the limit of large Re (3.17).

the sign function, and therefore need to only consider $|k| = 2\pi$. The resulting solution is

$$\breve{\Gamma}(k, s) = \frac{-\mathrm{i}\pi\,\mathrm{sgn}(k)\,\delta(|k| - 2\pi)}{s + \dfrac{8\pi^3}{Re\,s}\left(\sqrt{1 + \dfrac{Re\,s}{4\pi^2}} - 1\right)}. \tag{3.14}$$

To gain first a qualitative understanding of the surfactant dynamics, we examine the poles of (3.14). As illustrated in figure 2, the dynamics can be classified into one of five cases depending on the value of the Reynolds number:

(i) $Re \to 0$. In this limit, which describes dominantly viscous systems, the pole is $s = -\pi$. In the absence of the term on the left-hand side of (2.10), we have a Stokes flow. The complete solution for this case can be derived either directly from the governing equations or using the $Re \to 0$ limit of the solutions that have already been derived, which we present in § 3.2. The Stokes flow solution for a two-dimensional surface and a finite fluid depth is also available (Masoud & Shelley 2014).

(ii) $Re/(2\pi) < 1$, for which only one negative real pole exists.

(iii) $1 < Re/(2\pi) < 32/27$, for which two negative real poles exist.

(iv) $Re/(2\pi) > 32/27$, for which two complex conjugate poles with negative real parts exist.

(v) $Re \gg 1$. In this limit, equation (3.14) simplifies to

$$\breve{\Gamma}(k, s) = -\mathrm{i}\pi\,\mathrm{sgn}(k)\,\delta(|k| - 2\pi)\,\breve{\theta}(s), \tag{3.15}$$

where

$$\breve{\theta}(s) = \frac{1}{s + \dfrac{4\pi^2}{Re^{1/2}s^{1/2}}} \tag{3.16}$$

https://doi.org/10.1017/jfm.2016.507 Published online by Cambridge University Press

and has the two poles

$$s = 2\pi \left(\frac{Re}{2\pi}\right)^{-1/3} \left(-\frac{1}{2} \pm \mathrm{i}\frac{\sqrt{3}}{2}\right). \tag{3.17}$$

The poles are complex conjugates of each other and have negative real parts. Both the real and imaginary parts of the two poles decay to zero in proportion to $Re^{-1/3}$.

We focus now on the limit of large Re and invert the Laplace-domain solution, equation (3.15), back to the time domain. First, we note that

$$\begin{aligned} \breve{\theta}(s) &= \frac{1}{s + \dfrac{4\pi^2}{Re^{1/2}\, s^{1/2}}} \\ &= \frac{1}{3s^{1/2}} \left[\frac{1}{s^{1/2} - b_0 \dfrac{(2\pi)^{2/3}}{Re^{1/6}}} + \frac{1}{s^{1/2} - b_+ \dfrac{(2\pi)^{2/3}}{Re^{1/6}}} + \frac{1}{s^{1/2} - b_- \dfrac{(2\pi)^{2/3}}{Re^{1/6}}} \right], \end{aligned} \tag{3.18}$$

where $b_0 = -1$ and $b_\pm = (1 \pm \mathrm{i}\sqrt{3})/2$ are the three cube roots of -1. Of the three terms on the right, the first does not contribute a pole. The inverse Laplace transform of

$$F(s) = \frac{1}{\sqrt{s}\left(\sqrt{s} + \beta\right)}, \tag{3.19}$$

where β is a complex constant, is (Erdélyi *et al.* 1954, p. 234, equation (7))

$$\mathscr{L}^{-1}\{F(s)\} = f(t) = \exp(\beta^2 t)\mathrm{erfc}(\beta\sqrt{t}), \tag{3.20}$$

and we can use this to invert every term in (3.18). We thus obtain

$$\hat{\Gamma}(k, \tilde{t}) = -\mathrm{i}\pi\, \mathrm{sgn}(k)\, \delta(|k| - 2\pi)\, \theta(\tilde{t}) \tag{3.21}$$

and

$$\tilde{\Gamma}(\tilde{x}, \tilde{t}) = \sin(2\pi\tilde{x})\, \theta(\tilde{t}), \tag{3.22}$$

where the time-dependent component, $\theta(\tilde{t})$, which determines how the amplitude of the surfactant distribution decays over time, is

$$\theta(\tilde{t}) = \frac{1}{3} \sum_{n=0,+,-} \exp\left(b_n^2 \frac{(2\pi)^{4/3}}{Re^{1/3}} \tilde{t}\right) \mathrm{erfc}\left(-b_n \frac{(2\pi)^{2/3}}{Re^{1/6}} \sqrt{\tilde{t}}\right). \tag{3.23}$$

For any complex z, $\exp(\overline{z}^2)\mathrm{erfc}(\overline{z}) = \overline{\exp(z^2)\mathrm{erfc}(z)}$, where an overbar denotes the complex conjugate. Since $b_- = \overline{b_+}$, the $n = +$ and $n = -$ terms of the sum are complex conjugates of each other, and the sum of the three terms is real.

The decay of the variation in surfactant concentration resembles a damped oscillation, as shown in figure 3, but the amplitude of the variation becomes zero only three times and decays monotonically at late times. Determined numerically, the three roots $\tilde{t}_i$ of $\theta(\tilde{t})$ are $((2\pi)^{4/3}/Re^{1/3})\tilde{t}_i = 1.6452$, 5.7437 and 8.3765. Oscillations occur due to the inertia of the fluid that is set in motion by the surface stress distribution.

https://doi.org/10.1017/jfm.2016.507 Published online by Cambridge University Press

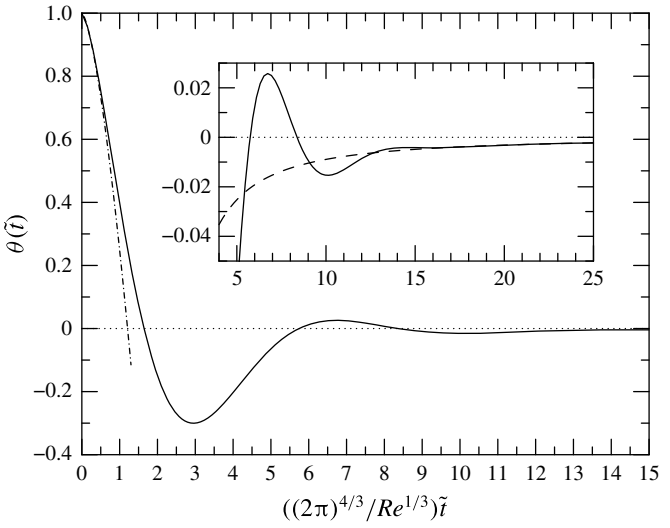


FIGURE 3. The decay over time of the amplitude of a sinusoidal surfactant concentration distribution at high Re (3.23). The early time behaviour (3.26) is shown with a dash-dotted line. The inset emphasizes the finite number of roots and the absence of sustained oscillation, with the late-time monotonic decay (3.24) shown as a dashed line.

Initially, regions with high surfactant concentration (lower surface tension) expand, while those with low concentration (higher tension) contract. When the surfactant distribution becomes uniform, first at $\tilde{t}_1$, the fluid continues to expand/contract the surfactant distribution, which now creates regions of locally low/high concentration. The surface stresses then reverse the upper layer of the flow, and the surfactant distribution decays again. The surfactant concentration overshoots the equilibrium two more times before gradually decaying to uniformity. The finite number of oscillations distinguishes this system from a typical damped oscillator.

Using $\exp(z^2)\mathrm{erfc}(z) \sim (1/z\sqrt{\pi})(1 - 1/2z^2)$ for large z, obtained from the first two terms of the asymptotic expansion of erfc (Olver *et al.* 2010, equation (7.12.1); DLMF 2015), we find that at late times, deviations in surfactant concentration decay monotonically according to the power law

$$\theta(\tilde{t}) \sim -\frac{1}{2\sqrt{\pi}}\left(\frac{(2\pi)^{4/3}}{Re^{1/3}}\tilde{t}\right)^{-3/2}. \tag{3.24}$$

This result is shown as the dashed line in the inset of figure 3. Two terms in the approximation are required because $1/b_0 + 1/b_+ + 1/b_- = 0$, which makes the contribution of the first term vanish in the sum in equation (3.23).

The factor on $\tilde{t}$ in the solution for the surfactant decay, equation (3.23), shows that in the large Re limit, the decay time scale is not the advective time scale $t^* = \lambda/u^*$. Instead, the surfactant decay time scale t^*_Γ is the cube root of the product of the viscous time scale $\rho\lambda^2/\mu$ and the square of the advective time scale $t^* = \lambda/u^*$:

$$t^*_\Gamma = t^* Re^{1/3} = \left(\frac{\rho\lambda^4\mu}{\alpha^2\bar{\Gamma}^2}\right)^{1/3} = \left(t^{*2}\frac{\rho\lambda^2}{\mu}\right)^{1/3}. \tag{3.25}$$

One may still interpret this as an advective time scale with characteristic velocity $u^*/Re^{1/3}$ instead of u^*.

https://doi.org/10.1017/jfm.2016.507 Published online by Cambridge University Press

The surfactant decay time scale also follows from a simple scaling argument. From the surfactant transport equation (3.1*a*), we have $\partial\tilde{\Gamma}/\partial\tilde{t} \sim \partial\tilde{u}_s/\partial\tilde{x} \sim \tilde{u}_s$, and the surface stress boundary condition (2.8) provides $\partial\tilde{u}/\partial\tilde{y} \sim \partial\tilde{\Gamma}/\partial\tilde{x} \sim \tilde{\Gamma}$ for $\tilde{y} \to 0^+$. Making the approximation that $\partial\tilde{u}/\partial\tilde{y} \sim \tilde{u}_s/\tilde{\delta}$, where $\tilde{\delta} \ll 1$ is a boundary layer thickness that grows over time as $\tilde{\delta} \sim (\tilde{t}/Re)^{1/2}$ (this follows from the momentum equation (3.1*b*) and $Re\,\partial\tilde{u}/\partial\tilde{t} \sim \partial^2\tilde{u}/\partial\tilde{y}^2$), we obtain $\tilde{u}_s \sim \tilde{\Gamma}\tilde{\delta}$. It follows that $\partial\tilde{\Gamma}/\partial\tilde{t} \sim (\tilde{t}/Re)^{1/2}\tilde{\Gamma}$, and scaling time by $Re^{-1/3}$ eliminates dependence on Re. This result also indicates that at early times $\log\tilde{\Gamma} \sim \tilde{t}^{3/2}/Re^{1/2}$, consistent with a series expansion of equation (3.23) about $\tilde{t} = 0$, which yields

$$\theta(\tilde{t}) = 1 - \frac{4}{3\sqrt{\pi}}\left(\frac{(2\pi)^{4/3}}{Re^{1/3}}\tilde{t}\right)^{3/2} \tag{3.26}$$

to leading order in $\tilde{t}$.

3.2. *Stokes flow limit*

In the Stokes flow limit, i.e. $Re \to 0$, of (2.10), the subsurface flow decays exponentially without oscillation (see also Masoud & Shelley 2014). In this limit, the Laplace-domain solution for the surfactant evolution simplifies to

$$\breve{\Gamma}(k, s) = \frac{1}{s + \pi}\hat{\Gamma}_0(k), \tag{3.27}$$

and inversion provides

$$\hat{\Gamma}(k, \tilde{t}) = \exp(-\pi\tilde{t})\hat{\Gamma}_0(k). \tag{3.28}$$

Furthermore, we obtain

$$\breve{p}(k, \tilde{y}, s) = \breve{p}_0(k, s)\ \exp(-|k|\tilde{y}), \tag{3.29a}$$

$$\breve{u}(k, \tilde{y}, s) = -\frac{\mathrm{i}}{2k}\breve{p}_0(k, s)\ \exp(-|k|\tilde{y})\ (|k|\tilde{y} - 1), \tag{3.29b}$$

$$\breve{v}(k, \tilde{y}, s) = \tfrac{1}{2}\breve{p}_0(k, s)\,\tilde{y}\exp(-|k|\tilde{y}), \tag{3.29c}$$

and the full time-domain solution for the initial condition $\tilde{\Gamma}_0(\tilde{x}) = \sin(2\pi\tilde{x})$ follows as

$$\tilde{\Gamma}(\tilde{x}, \tilde{t}) = \sin(2\pi\tilde{x})\exp(-\pi\tilde{t}), \tag{3.30a}$$

$$\tilde{u}(\tilde{x}, \tilde{y}, \tilde{t}) = -\tfrac{1}{2}\cos(2\pi\tilde{x})(1 - 2\pi\tilde{y})\exp(-2\pi\tilde{y})\exp(-\pi\tilde{t}), \tag{3.30b}$$

$$\tilde{v}(\tilde{x}, \tilde{y}, \tilde{t}) = -\tfrac{1}{2}\sin(2\pi\tilde{x})(2\pi\tilde{y})\exp(-2\pi\tilde{y})\exp(-\pi\tilde{t}), \tag{3.30c}$$

$$\tilde{p}_0(\tilde{x}, \tilde{t}) = -2\pi\sin(2\pi\tilde{x})\exp(-\pi\tilde{t}). \tag{3.30d}$$

The structure of the flow, which consists of periodic vertically stretched vortices, is illustrated in figure 4. As the solution shows, the surfactant decay time scale in the Stokes flow limit is the advective time scale chosen in the initial non-dimensionalization.

3.3. *Developing flow under a steady surfactant distribution*

To highlight how the time scale of the coupled transient problem differs from the advective and viscous time scales, we consider briefly a simpler problem: the response of the fluid to a sudden and sustained change in surfactant distribution. In contrast, the

https://doi.org/10.1017/jfm.2016.507 Published online by Cambridge University Press

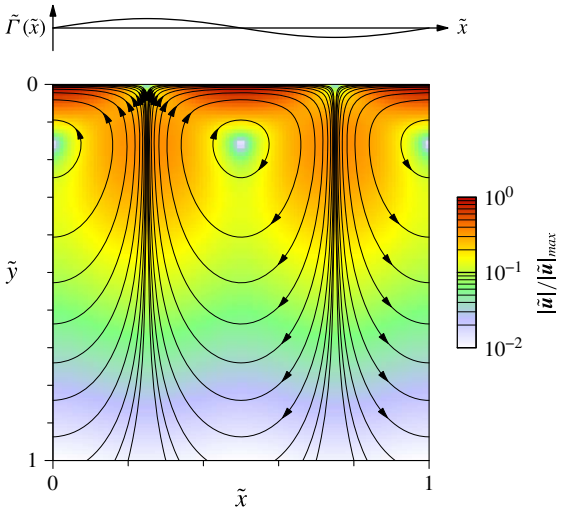


FIGURE 4. (Colour online) Stokes flow solution for the initial surfactant distribution $\tilde{\Gamma}_0(\tilde{x}) = \sin(2\pi\tilde{x})$ in the subdomain $[0, 1] \times [0, 1]$ of the semi-infinite domain. The structure of the flow remains constant as it decays exponentially.

surfactant distribution in the coupled problem is initially changed and then allowed to evolve over time. Specifically, we consider the response of a motionless fluid to $\tilde{\Gamma}(\tilde{x}, \tilde{t}) = \sin(2\pi\tilde{x})H(\tilde{t})$ where $H(\cdot)$ is the Heaviside step function. For this condition, we have

$$\hat{\Gamma}(k, \tilde{t}) = -\mathrm{i}\pi\,\mathrm{sgn}(k)\,\delta(|k| - 2\pi)\,H(\tilde{t}), \quad \breve{\Gamma}(k, s) = -\frac{\mathrm{i}\pi}{s}\,\mathrm{sgn}(k)\,\delta(|k| - 2\pi). \quad (3.31a,b)$$

Using (3.9*a*) and (3.10), the Laplace-domain solution for the surface speed is

$$\breve{u}(k, 0, s) = -\frac{4\pi^3}{Re\,s^2}\left(\sqrt{1 + \frac{Re\,s}{4\pi^2}} - 1\right)\delta(|k| - 2\pi), \quad (3.32)$$

and upon inverting the Laplace (Erdélyi *et al.* 1954) and Fourier transforms, we obtain the time-domain solution

$$\tilde{u}(\tilde{x}, 0, \tilde{t}) = -\cos(2\pi\tilde{x})\left[\frac{1}{2}\,\mathrm{erf}\left(\sqrt{\tilde{t}'}\right) - \tilde{t}'\,\mathrm{erfc}\left(\sqrt{\tilde{t}'}\right) + \sqrt{\frac{\tilde{t}'}{\pi}}\exp(-\tilde{t}')\right], \quad (3.33)$$

where $\tilde{t}' = 4\pi^2\tilde{t}/Re$. This solution is a monotonic rise in time to a steady state. The effect of Re here is a rescaling of time. The time scale for the development of a flow under a steady stress distribution is the viscous time scale $\rho\lambda^2/\mu$ in contrast to the advective time scale t^* of the coupled problem in the Stokes flow limit and t_Γ^* in the high Re limit.

4. Numerical results

We now investigate numerically the situations not addressed by the analytical cases, specifically large-amplitude variation in Γ and behaviour at intermediate Re. We use a semi-implicit spectral finite difference method in the vorticity–streamfunction form

https://doi.org/10.1017/jfm.2016.507 Published online by Cambridge University Press

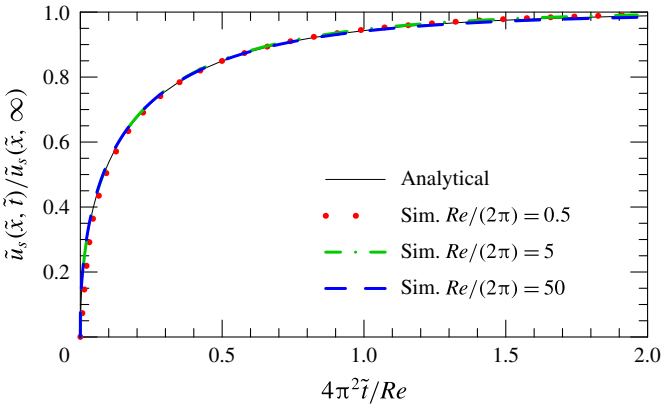


FIGURE 5. (Colour online) Comparison of the analytical solution for the development of the surface flow due to a constant sinusoidal surfactant distribution, equation (3.33), and simulations with $\varepsilon = 0.1$ and $Re/(2\pi) = 0.5$, 5 and 50. The flow evolves in the same way for all $\tilde{x}$.

(for details see appendix A). The approach is similar to that followed for the analytical solution but retains the nonlinear terms. A Fourier transform is used in the x direction, and second-order central finite differences are used in the y direction. The height of the simulation domain is finite, and the boundary condition for the vorticity on the no-slip boundary is applied using Thom's formula (Thom 1933). Integration in time is performed with the second-order Adams–Bashforth method after an initial explicit Euler time step. The resolution of the simulations is 64 points in the x direction and 257 in y for a domain with a height that is double its width. This aspect ratio is judged to be sufficiently high to approximate a semi-infinite domain because in the worst case of Stokes flow, the flow speed for the fundamental mode in a semi-infinite domain decays by four orders of magnitude within this depth. The spatial resolution in y is twice the resolution in x, chosen to resolve the flow near the surface. Unless specified otherwise, the initial condition is $\tilde{\Gamma}_0(\tilde{x}) = \sin(2\pi\tilde{x})$.

4.1. *Steady surfactant distribution*

As a benchmark, we examine first the transient solution for the flow developing from rest under a steady surfactant distribution, i.e. $\Gamma(x, t) = \Gamma_0(x)$ for $t > 0$. The computed surface speed as a function of time, shown in figure 5 for $Re/(2\pi) = 0.5$, 5, and 50 with $\varepsilon = 0.1$, agrees well with the analytical solution, equation (3.33). Though not shown, deviation from the analytical solution begins with $\varepsilon Re/(2\pi) \approx 10$ due to the nonlinear term in (2.10) that was neglected in the derivation of the analytical solution.

4.2. *Small* ε

Simulations of the full transient problem with decaying small-amplitude ($\varepsilon \to 0$) variations in the surfactant concentration and high Pe_s are shown in figure 6. In the limits of small and large Re, the numerical results approach the corresponding analytical solutions. For intermediate Re, the simulation results were compared with numerical inversion of the Laplace-domain solution (3.14). Since the simulations

https://doi.org/10.1017/jfm.2016.507 Published online by Cambridge University Press

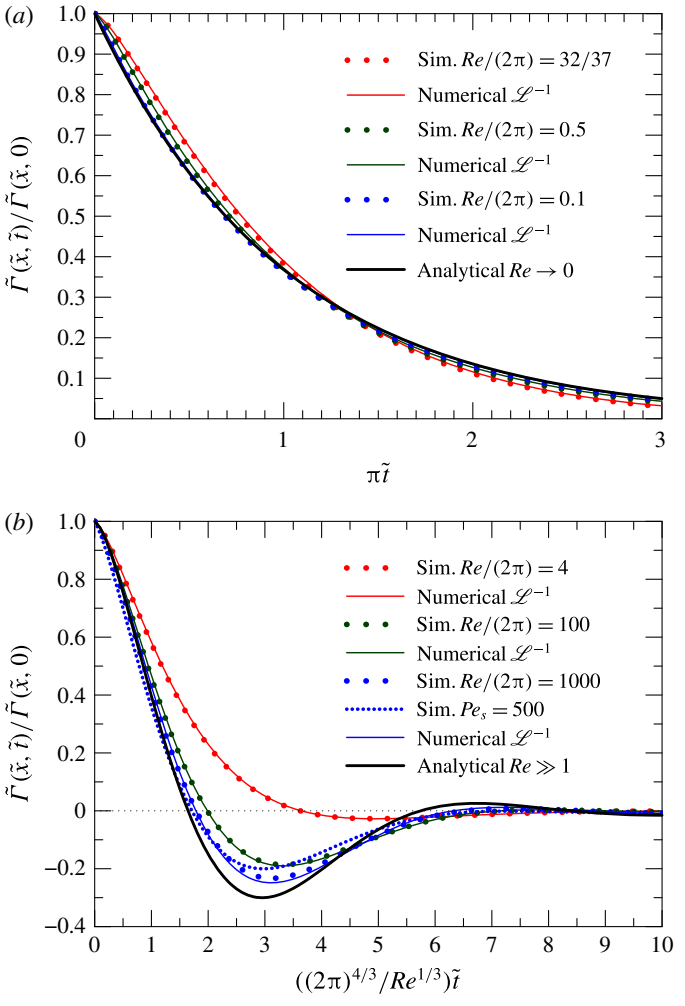


FIGURE 6. (Colour online) Numerical and analytical solutions for the decay of small variations in the surfactant concentration with (*a*) $Re/(2\pi) \leqslant 32/27$ and (*b*) $Re/(2\pi) > 32/27$. The dotted curves show the simulation results (with $\varepsilon = 0.01$), the coloured solid lines show numerical inversion of the Laplace domain solution (3.13), and the solid black lines show the analytical solutions ((3.28) for $Re \to 0$ and (3.23) for $Re \gg 1$). The curves with large dots were computed with sufficiently high Pe_s that diffusion is negligible ($Pe_s = 1000$ in (*a*) and in (*b*) $Pe_s = 1587$, 4641 and 10 000 for $Re/(2\pi) = 4$, 100 and 1000, respectively), while the curve with smaller dots in (*b*) shows the computed result for $Re/(2\pi) = 1000$ with $Pe_s = 500$.

include the surfactant diffusion term, a sufficiently large value of Pe_s is required to keep diffusion negligible. The choice of Pe_s must ensure that the diffusion time scale is significantly longer than the surfactant decay time scale, which is not necessarily the advection time scale used to define Pe_s. In the limit of low Re, we require

$$\frac{\lambda^2}{D_s} \gg \frac{t^*}{\pi} \Rightarrow Pe_s \gg 1, \tag{4.1}$$

https://doi.org/10.1017/jfm.2016.507 Published online by Cambridge University Press

whereas in the high Re limit the requirement is

$$\frac{\lambda^2}{D_s} \gg \frac{Re^{1/3}t^*}{(2\pi)^{4/3}} \Rightarrow \frac{(2\pi)^{4/3}}{Re^{1/3}}Pe_s \gg 1, \tag{4.2}$$

which follows from (3.25). While a fixed high Pe_s is suitable at low Re, in which case the surfactant decay time scale is the advection time scale, Pe_s must be scaled in proportion to $Re^{1/3}$ for high Re. The simulations in figure 6(*a*) all had $Pe_s = 1000$, while those in figure 6(*b*) were performed with $Pe_s = 1587$, 4641 and 10 000 for $Re/(2\pi) = 4$, 100 and 1000, respectively. For these values, $(Re/(2\pi))^{-1/3}Pe_s = 1000$. Good agreement in all cases with the Laplace-domain solution for infinite Pe_s indicates that these choices of Pe_s are satisfactory to suppress the effects of diffusion. For comparison, a simulation with $Pe_s = 500$ and $Re/(2\pi) = 1000$ is also shown in figure 6. At this lower Pe_s, agreement with the high Pe_s solution is still reasonable. Though not shown in figure 6, the surfactant distribution continues to decay faster as Pe_s is decreased further. With $Pe_s = 10$, the minimum becomes -0.01 at $[(2\pi)^{4/3}/Re^{1/3}]\tilde{t} \approx 1.5$.

The evolution of the flow structure at $Re/(2\pi) = 100$ and $\varepsilon = 0.01$ is illustrated in figure 7. As mentioned earlier, the oscillations in the surfactant concentration occur due to the inertia of the flow when the surfactant concentration first becomes uniform. During the initial decay in the amplitude of the surfactant variation, its first zero crossing, and subsequent growth, the flow structure consists of a row of counter-rotating vortices that penetrate deeper into the fluid layer over time. A second layer of vortices forms above the initial layer when the first peak in amplitude (of the opposite sign to the initial condition) is reached. The change in sign of the surface stress therefore reverses the motion of the surfactant and creates this new layer of vortices rather than stopping and reversing the initial vortex layer. The flow structure alternates between having one and two layers of vortices until the third and final peak in amplitude. The flow and surfactant concentration variation then decay monotonically to zero with two rows of vortices present. The development of the flow for $Re/(2\pi) = 100$ is representative of the structure seen in the oscillatory decay regime ($Re/(2\pi) > 32/27$). With increasing Re, however, the vortices are compressed vertically.

4.3. *Initial conditions with multiple modes*

Due to the linearity of the governing equations in the limit of small ε, the solutions for arbitrary periodic initial surfactant distributions can be constructed by superposition of the solutions for single modes. Expanding $\tilde{\Gamma}_0(\tilde{x})$ for $\tilde{x} \in [0, 1]$ in a Fourier series as $\sum_{n=1}^{\infty} a_n \sin(2\pi n\tilde{x} + \phi_n)$, we see that the solution will consist of the single-mode solutions for wavelengths $\lambda_n = \lambda_1/n$ where λ_1 is the wavelength of the fundamental mode. These modes have corresponding Reynolds numbers $Re_n = Re_1/n$ and time scales $t_n^* = t_1^*/n$. The fundamental mode decays slowest, as shown in figure 8 for (*a*) an initial distribution that has two modes and (*b*) one that is random. For the simulation with two modes, Pe_s was chosen as 20 800 to satisfy equation (4.2) for the $n = 3$ mode; for the random distribution, $Pe_s = 10\,000$ for the fundamental mode. The evolution of the random distribution shows that when the fundamental mode reaches its first zero, the third and higher modes are effectively negligible because the solution at this time is bounded by the amplitude of the second mode.

https://doi.org/10.1017/jfm.2016.507 Published online by Cambridge University Press

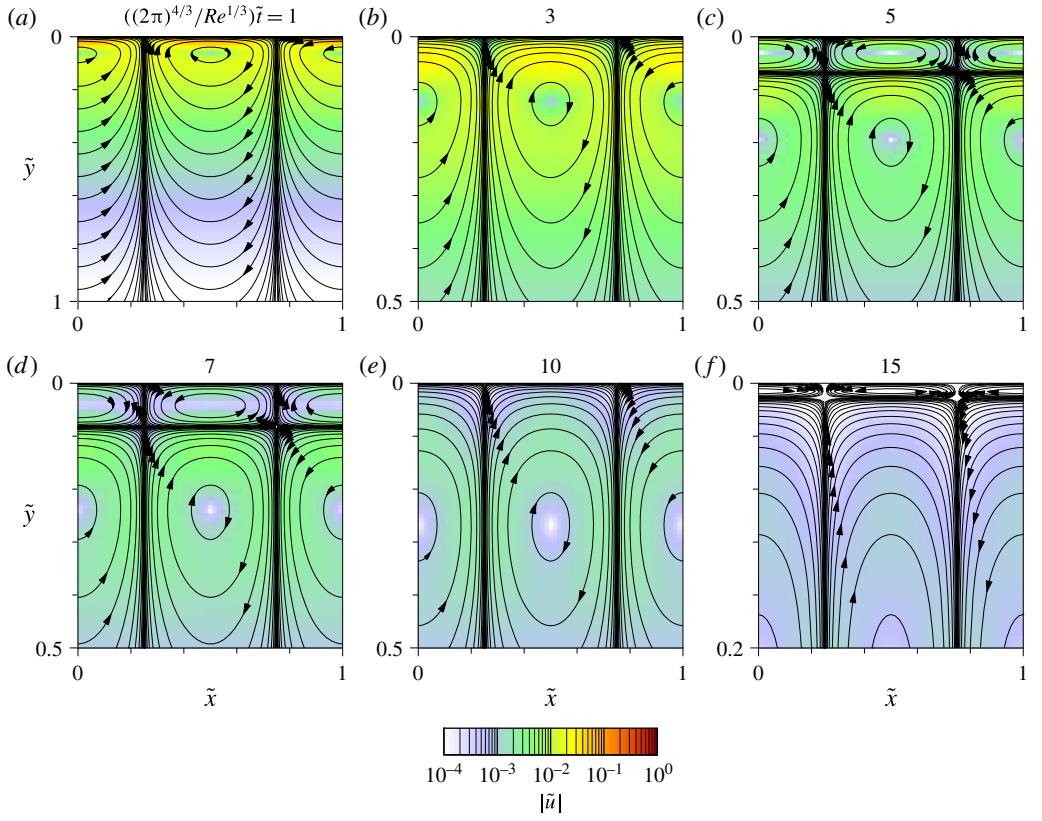


FIGURE 7. (Colour online) Evolution of the flow structure at $Re/(2\pi)=100$ and $\varepsilon=0.01$ in the upper half (*a*), quarter (*b–e*), and fifth (*f*) of the simulated domain. The colour indicates the flow speed, and a logarithmic colour scale is used for convenience. Time proceeds from (*a*) to (*f*). Different ranges of the vertical axes in (*a*) and (*f*) are used to emphasize the structure of the flow.

4.4. *Finite* ε

For small ε, the portions of the surface with positive and negative deviation from the mean surfactant concentration evolve symmetrically, and this case is described by the analytical and Laplace-domain solutions. The simulations in figure 9 show the asymmetry in the evolution of the surfactant as ε increases to one, which is its upper bound since negative concentrations are inadmissible. While the results for $\varepsilon=0.01$ match the $\varepsilon\to 0$ solutions, the region with positive $\tilde{\Gamma}$ initially widens and decays faster for higher ε with low Re (figure 9*a*), the region with negative $\tilde{\Gamma}$ narrows, and the concentration profile sharpens around the minimum. These effects are due to the nonlinear term in (2.9), which accelerates the decrease of $\tilde{\Gamma}$ near its maximum, makes $\partial\tilde{\Gamma}/\partial\tilde{t}$ non-zero where initially $\tilde{\Gamma}\approx 0$, and decreases $\partial\tilde{\Gamma}/\partial\tilde{t}$ near the minimum $\tilde{\Gamma}$. In fact, as will be described in greater detail for higher Re, the convective term vanishes at the minimum $\tilde{\Gamma}$ as $\varepsilon\to 1$ leaving only diffusion to drive changes in concentration there.

At the higher Re, for which oscillations occur (figure 9*b*,*c*), the effects of increasing ε are more complex because of the nonlinear terms in both the surfactant evolution

https://doi.org/10.1017/jfm.2016.507 Published online by Cambridge University Press

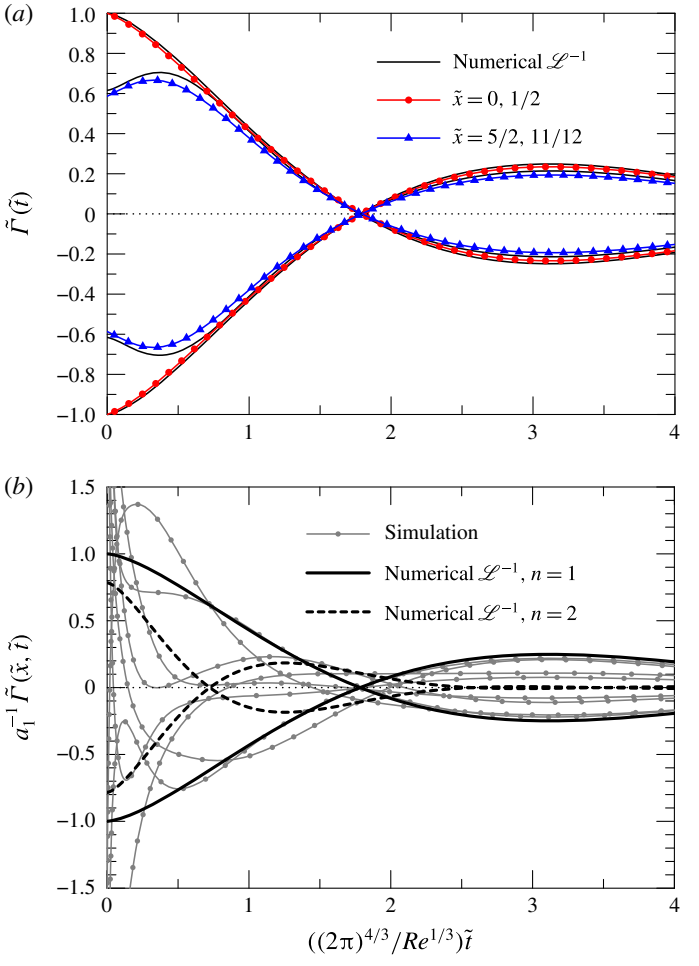


FIGURE 8. (Colour online) The decay of initial surfactant distributions with multiple modes. The time axis is scaled using the Reynolds number for the fundamental mode, Re_1, with $Re_1/(2\pi) = 1000$ and $\varepsilon = 0.01$ for both cases. In (*a*), the initial condition is $\tilde{\Gamma}_0(\tilde{x}) = \cos(2\pi\tilde{x}) + (1/4)\sin(6\pi\tilde{x})$. The numerical solutions (coloured lines with symbols) are compared with numerical inversion of the Laplace-domain solution (solid black lines) at $\tilde{x} = 0$, 5/12, 1/2 and 11/12. In (*b*), $\tilde{\Gamma}_0$ is a random value from $[-1, 1]$ at each point in the simulated domain. The concentrations are shown at positions $\tilde{x}$ that are multiples of 1/8 (grey lines with dots), and they are scaled by the magnitude a_1 of the fundamental mode in the initial condition. The black lines show the decay of the first ($n = 1$, solid) and second ($n = 2$, dashed) modes in the initial distribution obtained by numerical inversion of the Laplace-domain solution and evaluated at the positions of maximum amplitude for each mode.

and fluid flow. At early times ($[(2\pi)^{4/3}/Re^{1/3}]\tilde{t} < 1$), the behaviour is similar to that with lower *Re*. Unlike at lower *Re*, the concentration at the minimum then begins to increase faster, and for $\varepsilon = 1$, the growth rate exceeds that in the immediately adjacent regions, and a local maximum and two adjacent minima form in the surfactant concentration. This local maximum is more pronounced and occurs earlier at the

https://doi.org/10.1017/jfm.2016.507 Published online by Cambridge University Press

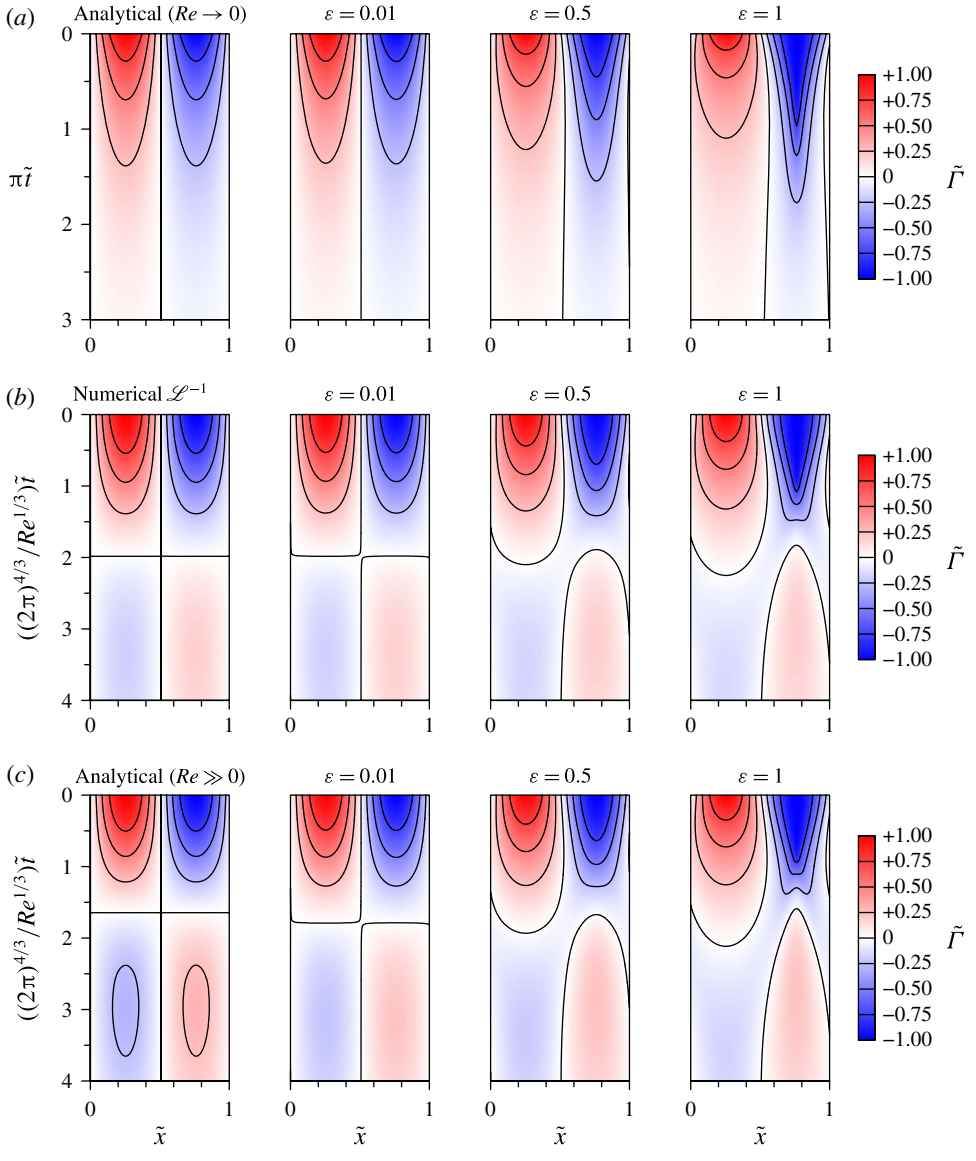


FIGURE 9. (Colour online) Evolution of the surfactant concentration in the limit $\varepsilon \to 0$ (analytical solutions or numerical inversion of Laplace-domain solution) and numerical solutions for finite-amplitude variation in concentration ($\varepsilon = 0.01$, 0.5 and 1) at (*a*) $Re/(2\pi) = 0.1$, (*b*) 100 and (*c*) 1000.

highest Re. From $[(2\pi)^{4/3}/Re^{1/3}]\tilde{t} \approx 1.5$ to 2, a temporary doubling in the spatial frequency of the concentration profile is evident.

The asymmetry in the evolution of the surfactant concentrations at the locations of the initial minimum and maximum is emphasized in figure 10. The most significant change in the dynamics with increasing ε is the emergence of a delay in the growth of the concentration from $\tilde{\Gamma} = -1$. In figure 9, this was seen as a narrowing of the region with negative $\tilde{\Gamma}$. For ε approaching sufficiently close to one, the advective terms in

https://doi.org/10.1017/jfm.2016.507 Published online by Cambridge University Press

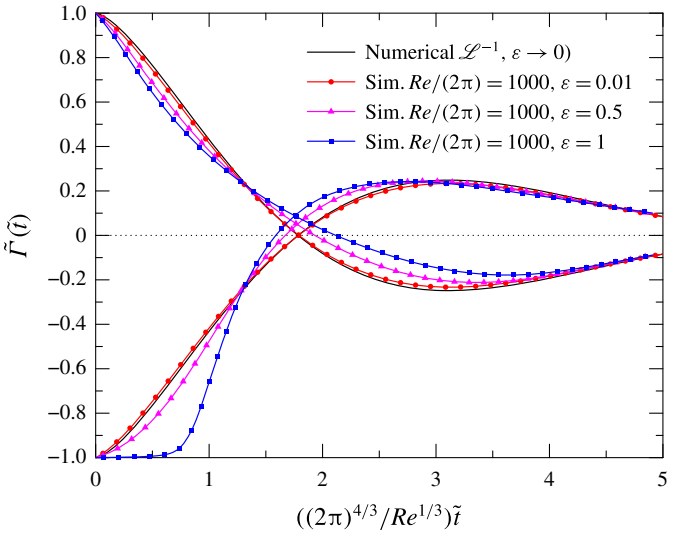


FIGURE 10. (Colour online) Asymmetry in the decay of the surfactant concentration from its maximum and minimum values at $Re/(2\pi) = 1000$, $Pe_s = 10\,000$, and several ε. The solid black line shows the numerical inversion of the Laplace-domain solution for the limit of $\varepsilon \to 0$, equation (3.14).

the surfactant dynamics become negligible for any Pe_s, leaving only diffusion to drive changes in $\tilde{\Gamma}$ at early times. The diffusive flux that determines the duration of the initial delay depends on the initial concentration profile and the developing flow, which sharpens the profile, increasing the flux. The dominance of the diffusive term persists until $\tilde{\Gamma}$ increases sufficiently that the advective terms take over. Due to the effect of diffusion on the initial delay, the surfactant evolution for high ε is expected to depend on Pe_s.

4.5. *Parameters for physical systems*

Where do typical physical systems lie in the dimensionless parameter space and how would they behave? Consider an aqueous surfactant solution with a clean surface tension γ_0 of 72 mN m^{-1} and 10 % variation in tension around a mean of 50 mN m^{-1}. Using $\rho = 1000$ kg m^{-3} and $\mu = 1$ mPa s, we obtain $Re = 2.2 \times 10^4$ for a millimetre-scale variation in surface tension. The advective time scale is 45 μs. Assuming a diffusivity of the order of 10^{-9} m^2 s^{-1}, which is typical of small solute molecules, the diffusive time scale is $\lambda^2/D_s = 10^3$ s and $Pe_s = 2.2 \times 10^7$. This system is clearly in the high Re limit and the surfactant decay time scale is 1.3 ms, much shorter than the diffusive time scale. For centimetre-scale variation, $Re = 2.2 \times 10^5$, the advective time scale is 0.45 ms, the diffusive time scale is 10^5 s, $Pe_s = 2.2 \times 10^8$ and the surfactant decay time scale is 27 ms. For both these sample sets of parameters, the surfactant decay time scales are significantly shorter than the diffusion time scales, satisfying the key assumption in the modelling that Pe_s is large and diffusion can be neglected. The diffusivities of larger solute molecules can be up to several orders of magnitude lower, such as 10^{-10} m^2 s^{-1} for sodium dodecyl sulphate, and values of Pe_s for such solutes would be correspondingly higher. Considering that Schmidt numbers $Sc_s = \mu/(\rho D_s) = Pe_s/Re$ for aqueous systems are typically $O(1000)$, the

https://doi.org/10.1017/jfm.2016.507 Published online by Cambridge University Press

assumption of high Pe_s is reasonable for the oscillatory surfactant decay regime in which Re exceeds one. The effects of diffusion need to be included for lower Re, however, unless the system has a higher Sc_s. The high Re of the sample systems, which exceed those considered in this paper for $\varepsilon > 0$, motivate further study of nonlinear phenomena at high Re and finite ε, in particular the limit $\varepsilon \to 1$.

5. Conclusions

We have presented analytical solutions for the decay of small-amplitude variations in the concentration of an insoluble surfactant on an initially motionless and infinitely deep layer of a Newtonian liquid. Surfactant diffusion was neglected in the analytical solutions. While the surfactant decays monotonically (and exponentially) in the Stokes flow limit, for unsteady Stokes flow at higher Re, the amplitude of the surfactant concentration distribution oscillates, changing sign three times before decaying monotonically at late times as $t^{-3/2}$. A unique feature of the dynamics of this system is this finite number of oscillations, which distinguishes it from a typical damped simple harmonic oscillator. During the oscillations, the structure of the flow below the surface alternates between one and two layers of counter-rotating vortices. The origin of the oscillations is the inertia of the flow induced by the initial surface Marangoni stress distribution, which drives the surfactant concentration beyond a uniform equilibrium distribution. The analytical solution for the surfactant concentration in the limit of large Re reveals that the time scale for surfactant decay (and oscillation) is the cube root of the product of the viscous time scale and the square of the advective time scale. In contrast, at low Re the decay time scale is simply the advective time scale.

We used a hybrid spectral–finite difference method to examine the nonlinear problem of finite-amplitude (ε) variations in surfactant concentration in the limit of high surface Péclet number. Increases in ε create an asymmetry in the evolution of regions with above- and below-average surfactant concentration. The portion of the surface with a positive deviation from the mean initially widens and decays faster than it would for lower ε, while growth in the portion with a negative deviation is delayed. In the limit $\varepsilon \to 1$, the delay is significant and is caused by diffusion of the surfactant dominating over advection at early times in the vicinity of the minimum (near zero) concentration. At high Re, the rapid growth after the delay creates an additional local maximum and two adjacent minima in the concentration profile, which contribute higher-frequency components to the surfactant distribution than the initial fundamental frequency.

Since typical aqueous systems would have higher Re than those we considered at present (see § 4.5), nonlinear phenomena in the behaviour of surfactants at higher Re with large-amplitude variations in concentration deserve further attention (i.e. the limit of $\varepsilon \to 1$ and $Re \gg 1$). A wide variety of additional physical and chemical phenomena could also be included in the model to examine their effects on the evolution and oscillation of surfactant distributions. Possibilities include soluble surfactants, confinement (i.e. finite height of the fluid layer), a deforming surface, two viscous fluids, reactions and surfactant adsorption/desorption at the interface and the evolution of two-dimensional surfactant patterns on a three-dimensional fluid domain. In physiological systems, which can be significantly more viscous than higher purity aqueous systems, the effects of non-Newtonian rheology, such as shear thinning, could also be considered. A better understanding of surfactant and flow dynamics on interfaces could be used to enhance heat and mass transfer and study the motion of individual organisms and inanimate particles on interfaces, as well as the collective motion of many such particles.

https://doi.org/10.1017/jfm.2016.507 Published online by Cambridge University Press

Acknowledgement

O.S. thanks the Natural Sciences and Engineering Research Council of Canada (NSERC) for a postdoctoral fellowship.

Appendix A. Numerical method

The transport equation for the surfactant concentration, including diffusion, on a non-deforming planar surface is:

$$\frac{\partial \Gamma}{\partial t} + \nabla_s \cdot (\Gamma \boldsymbol{u}_s) = D_s \nabla_s^2 \Gamma, \tag{A 1}$$

where $\boldsymbol{u}_s(\boldsymbol{x}, t) = \boldsymbol{u}(\boldsymbol{x}, y = 0, t)$, $\boldsymbol{x}$ is the position on the plane and y is perpendicular to it and extends into the adjacent fluid. Since surfactant is transported only in one direction, x, in the plane, the equation above reduces to

$$\frac{\partial \Gamma}{\partial t} + \frac{\partial}{\partial x}(\Gamma u_s) = D_s \frac{\partial^2 \Gamma}{\partial x^2}. \tag{A 2}$$

Taking the Fourier transform of both sides in x we have

$$\frac{\partial \hat{\Gamma}}{\partial t} + \mathrm{i}k\widehat{u_s \Gamma} = -D_s k^2 \hat{\Gamma}, \tag{A 3}$$

which can also be written as

$$\frac{\partial}{\partial t}[\exp(D_s k^2 t)\hat{\Gamma}] = -\exp(D_s k^2 t)\mathrm{i}k\widehat{u_s \Gamma}. \tag{A 4}$$

In the discrete form, the first time step uses the first-order Euler method:

$$\hat{\Gamma}^{m+1} = \exp(-D_s k^2 \Delta t)[\hat{\Gamma}^m - \mathrm{i}k\Delta t\widehat{u_s \Gamma}^m]. \tag{A 5}$$

All subsequent time steps use the second-order Adams–Bashforth method:

$$\hat{\Gamma}^{m+1} = \exp(-D_s k^2 \Delta t)\left[\hat{\Gamma}^m - \frac{\mathrm{i}k\Delta t}{2}(3\widehat{u_s \Gamma}^m - \exp(-D_s k^2 \Delta t)\widehat{u_s \Gamma}^{m-1})\right]. \tag{A 6}$$

While analytical solutions were obtained for a semi-infinite two-dimensional system, a finite domain size (W in x and H in y) is used for the simulations. The Navier–Stokes equations for the fluid in the bulk can be written in the vorticity–streamfunction form as

$$\frac{\partial \omega}{\partial t} + \boldsymbol{u} \cdot \nabla \omega = \nu \nabla^2 \omega, \tag{A 7}$$

$$\nabla^2 \psi = \omega, \tag{A 8}$$

where $\nu = \mu/\rho$ and

$$u = \frac{\partial \psi}{\partial y}, \quad v = -\frac{\partial \psi}{\partial x}. \tag{A 9a,b}$$

The boundary conditions are

$$u(0, y) = u(W, y), \quad v(0, y) = v(W, y), \tag{A 10a,b}$$

$$\mu \frac{\partial u}{\partial y}(x, 0) = -\frac{\partial \gamma}{\partial x} = \alpha \frac{\partial \Gamma}{\partial x}, \quad v(x, 0) = 0, \quad u(x, H) = v(x, H) = 0. \tag{A 10c–e}$$

https://doi.org/10.1017/jfm.2016.507 Published online by Cambridge University Press

The domain is periodic in x, has a Marangoni stress distribution at $y=0$ and a no-slip wall at $y=H$. The boundary conditions for the vorticity and streamfunction are:

$$\omega(x,0)=\frac{\partial u}{\partial y}(x,0)=\frac{\alpha}{\mu}\frac{\partial \Gamma}{\partial x}, \tag{A 11a}$$

$$\omega(0,y)=\omega(W,y), \quad \frac{\partial \omega}{\partial x}(0,y)=\frac{\partial \omega}{\partial x}(W,y), \tag{A 11b,c}$$

$$\psi(x,0)=0, \quad \psi(x,H)=0, \quad \frac{\partial \psi}{\partial y}(x,H)=0, \tag{A 11d–f}$$

$$\psi(0,y)=\psi(W,y), \quad \frac{\partial \psi}{\partial x}(0,y)=\frac{\partial \psi}{\partial x}(W,y). \tag{A 11g,h}$$

Taking the Fourier transform in x we have

$$\frac{\partial \hat{\omega}}{\partial t}+\widehat{\boldsymbol{u}\cdot\boldsymbol{\nabla}\omega}=\nu\left(\frac{\partial^2\hat{\omega}}{\partial y^2}-k^2\hat{\omega}\right), \tag{A 12a}$$

$$\frac{\partial^2\hat{\psi}}{\partial y^2}-k^2\hat{\psi}=\hat{\omega}, \tag{A 12b}$$

$$\hat{\omega}(k,0)=\mathrm{i}k\frac{\alpha}{\mu}\hat{\Gamma}, \tag{A 12c}$$

$$\hat{\psi}(x,0)=0, \quad \hat{\psi}(x,H)=0, \tag{A 12d,e}$$

which can be written in discrete form as (skipping the use of first-order Euler integration for the first time step):

$$\hat{\omega}_n^{m+1}-\frac{\nu\Delta t}{2}\left(\frac{\hat{\omega}_{n+1}^{m+1}-2\hat{\omega}_n^{m+1}+\hat{\omega}_{n-1}^{m+1}}{(\Delta y)^2}-k^2\hat{\omega}_n^{m+1}\right)$$
$$=\hat{\omega}_n^{m}+\frac{\nu\Delta t}{2}\left(\frac{\hat{\omega}_{n+1}^{m}-2\hat{\omega}_n^{m}+\hat{\omega}_{n-1}^{m}}{(\Delta y)^2}-k^2\hat{\omega}_n^{m}\right)-\frac{\Delta t}{2}(3\widehat{\boldsymbol{u}\cdot\boldsymbol{\nabla}\omega}^{\,m}-\widehat{\boldsymbol{u}\cdot\boldsymbol{\nabla}\omega}^{\,m-1}), \tag{A 13a}$$

$$\hat{\omega}_1^{m+1}=\mathrm{i}k\frac{\alpha}{\mu}\hat{\Gamma}^{m+1}, \quad \hat{\omega}_N^{m+1}=\frac{2}{(\Delta y)^2}\hat{\psi}_{N-1}^{m+1} \quad \text{(Thom's formula (Thom 1933))}, \tag{A 13b,c}$$

$$[2+(\Delta y)^2k^2]\hat{\psi}_n^{m+1}-\hat{\psi}_{n+1}^{m+1}-\hat{\psi}_{n-1}^{m+1}=-(\Delta y)^2\hat{\omega}_n^{m+1}, \tag{A 13d}$$

$$\hat{\psi}_1^{m+1}=0, \quad \hat{\psi}_N^{m+1}=0, \tag{A 13e,f}$$

$$\hat{u}_n^{m+1}=\frac{\hat{\psi}_{n+1}^{m+1}-\hat{\psi}_{n-1}^{m+1}}{2\Delta y}, \tag{A 13g}$$

$$\hat{u}_s{}^{m+1}=\hat{u}_1^{m+1}=\frac{2\hat{\psi}_2^{m+1}-(\Delta y)^2\hat{\omega}_1^{m+1}}{2\Delta y}, \quad \hat{u}_N^{m+1}=0, \tag{A 13h,i}$$

$$\hat{w}_n^{m+1}=-\mathrm{i}k\hat{\psi}_n^{m+1}, \tag{A 13j}$$

$$\hat{w}_1^{m+1}=0, \quad \hat{w}_N^{m+1}=0. \tag{A 13k,l}$$

Here N is the number of points in the y direction spaced by Δy, subscripts denote indices in the y direction, and superscripts denote time steps of size Δt. The dimensionless parameters in the simulations are

$$Pe_s=\frac{\alpha\bar{\Gamma}W}{\mu D_s}, \quad Re=\frac{\alpha\bar{\Gamma}W}{\mu\nu}, \quad \varepsilon=\frac{\Delta\Gamma}{\bar{\Gamma}}, \quad \mathcal{A}=\frac{H}{W}, \tag{A 14a–d}$$

where $\Delta\Gamma=\max(\Gamma)-\bar{\Gamma}$ is the amplitude of the variation in Γ, and $\mathcal{A}$ is the aspect ratio of the domain.

https://doi.org/10.1017/jfm.2016.507 Published online by Cambridge University Press

Appendix B. Derivations

We provide here the derivations of the main results in the paper with additional details. We start with the non-dimensional form of the flow equation

$$Re\frac{\partial \tilde{\boldsymbol{u}}}{\partial \tilde{t}} = -\tilde{\boldsymbol{\nabla}}\tilde{p} + \tilde{\nabla}^2\tilde{\boldsymbol{u}}, \tag{B 1}$$

and take its divergence to obtain

$$\tilde{\nabla}^2\tilde{p} = 0. \tag{B 2}$$

Applying the Fourier transform,

$$-k^2\hat{p} + \frac{\partial^2\hat{p}}{\partial\tilde{y}^2} = 0, \tag{B 3}$$

and ensuring boundedness as $\tilde{y}\to\infty$, the solution for $k>0$ is

$$\hat{p}(k,\tilde{y},\tilde{t}) = \hat{p}_0(k,\tilde{t})\exp(-k\tilde{y}), \tag{B 4}$$

while for $k<0$ it is

$$\hat{p}(k,\tilde{y},\tilde{t}) = \hat{p}_0(k,\tilde{t})\exp(k\tilde{y}), \tag{B 5}$$

where the pressure along the surface is $\tilde{p}_0(\tilde{x},\tilde{t}) = \tilde{p}(\tilde{x},0,\tilde{t})$. Combining the two cases, we have

$$\hat{p}(k,\tilde{y},\tilde{t}) = \hat{p}_0(k,\tilde{t})\exp(-|k|\tilde{y}), \quad \breve{p}(k,\tilde{y},s) = \breve{p}_0(k,s)\exp(-|k|\tilde{y}). \tag{B 6a,b}$$

The $\tilde{y}$ component of the linearized momentum equation yields

$$Re\frac{\partial\tilde{v}}{\partial\tilde{t}} = -\frac{\partial\tilde{p}}{\partial\tilde{y}} + \frac{\partial^2\tilde{v}}{\partial\tilde{x}^2} + \frac{\partial^2\tilde{v}}{\partial\tilde{y}^2}, \tag{B 7a}$$

$$Re\frac{\partial\hat{v}}{\partial\tilde{t}} = -\frac{\partial\hat{p}}{\partial\tilde{y}} - k^2\hat{v} + \frac{\partial^2\hat{v}}{\partial\tilde{y}^2}. \tag{B 7b}$$

Taking the Laplace transform and using $\tilde{v}=0$ at $\tilde{t}=0$,

$$Re(s\breve{v} - \hat{v}(k,\tilde{y},0)) = |k|\breve{p}_0(k,s)\exp(-|k|\tilde{y}) - k^2\breve{v} + \frac{\partial^2\breve{v}}{\partial\tilde{y}^2}, \tag{B 8a}$$

$$\left(Re\,s + k^2\right)\breve{v} - \frac{\partial^2\breve{v}}{\partial\tilde{y}^2} = |k|\breve{p}_0(k,s)\exp(-|k|\tilde{y}). \tag{B 8b}$$

Retaining terms that are bounded as $\tilde{y}\to\infty$, the solution is

$$\breve{v}(k,\tilde{y},s) = \frac{|k|\breve{p}_0}{Re\,s}\exp(-|k|\tilde{y}) + \breve{A}\exp\left(-\tilde{y}\sqrt{k^2+Re\,s}\right), \tag{B 9}$$

where $\breve{A}(k,s)$ is unknown. Since $\tilde{v}=0$ at $\tilde{y}=0$, it follows that

$$\breve{v}(k,\tilde{y},s) = \frac{|k|\breve{p}_0}{Re\,s}\left[\exp(-|k|\tilde{y}) - \exp\left(-\tilde{y}\sqrt{k^2+Re\,s}\right)\right]. \tag{B 10}$$

Transforming the incompressibility constraint $\tilde{\boldsymbol{\nabla}}\cdot\tilde{\boldsymbol{u}}=0$, we find

$$\mathrm{i}k\breve{u} + \frac{\partial\breve{v}}{\partial\tilde{y}} = 0, \tag{B 11}$$

https://doi.org/10.1017/jfm.2016.507 Published online by Cambridge University Press

and substituting (B 10) we obtain

$$\breve{u}(k,\tilde{y},s)=\frac{\mathrm{i}k\breve{p}_0}{|k|Re\,s}\left[\sqrt{k^2+Re\,s}\exp\left(-\tilde{y}\sqrt{k^2+Re\,s}\right)-|k|\exp(-|k|\tilde{y})\right]. \tag{B 12}$$

In the Stokes flow limit $Re\to 0$, the solution is

$$\breve{p}(k,\tilde{y},s)=\breve{p}_0(k,s)\exp(-|k|\tilde{y}), \tag{B 13a}$$

$$\breve{u}(k,\tilde{y},s)=-\frac{\mathrm{i}\breve{p}_0}{2k}(|k|\tilde{y}-1)\exp(-|k|\tilde{y}), \tag{B 13b}$$

$$\breve{v}(k,\tilde{y},s)=\tfrac{1}{2}\breve{p}_0\tilde{y}\exp(-|k|\tilde{y}). \tag{B 13c}$$

The surface stress boundary condition is

$$\left.\frac{\partial\breve{u}}{\partial\tilde{y}}\right|_{\tilde{y}=0}=\mathrm{i}k\breve{\Gamma}, \tag{B 14}$$

which leads to

$$\breve{p}_0=-|k|\breve{\Gamma}. \tag{B 15}$$

Taking the Fourier and Laplace transforms of the surfactant evolution equation, we obtain

$$s\breve{\Gamma}-\hat{\Gamma}_0(k)+\mathrm{i}k\breve{u}_s=0, \tag{B 16}$$

and substituting (B 12) and (B 15) provides the solution for the evolution of the surfactant concentration:

$$\breve{\Gamma}(k,s)=\frac{1}{s+\dfrac{|k|^3}{Re\,s}\left(\sqrt{1+\dfrac{Re\,s}{k^2}}-1\right)}\hat{\Gamma}_0(k). \tag{B 17}$$

For large Re,

$$\frac{1}{s+\dfrac{|k|^3}{Re\,s}\left(\sqrt{1+\dfrac{Re\,s}{k^2}}-1\right)}\approx\frac{1}{s+\dfrac{k^2}{\sqrt{Re\,s}}}. \tag{B 18}$$

In the limit $Re\to 0$, we substitute (B 13b) instead of (B 12) into (B 16) and obtain

$$\breve{\Gamma}(k,s)=\frac{1}{s+\frac{1}{2}|k|}\hat{\Gamma}_0(k). \tag{B 19}$$

In this case,

$$\hat{\Gamma}(k,\tilde{t})=\hat{\Gamma}_0(k)\exp\left(-\tfrac{1}{2}|k|\tilde{t}\right), \tag{B 20a}$$

$$\hat{p}_0(k,\tilde{t})=-|k|\hat{\Gamma}(k,\tilde{t})=-|k|\,\hat{\Gamma}_0(k)\,\exp\left(-\tfrac{1}{2}|k|\tilde{t}\right). \tag{B 20b}$$

For the initial condition $\tilde{\Gamma}_0(\tilde{x})=\sin(2\pi\tilde{x})$, we have

$$\hat{\Gamma}_0(k)=-\mathrm{i}\pi\,\mathrm{sgn}(k)\,\delta(|k|-2\pi), \tag{B 21}$$

the solution for the surface pressure is

$$\hat{p}_0(k,\tilde{t})=\mathrm{i}\pi k\,\delta(|k|-2\pi)\exp\left(-\tfrac{1}{2}|k|\tilde{t}\right),\quad \tilde{p}_0(\tilde{x},\tilde{t})=-2\pi\sin(2\pi\tilde{x})\exp(-\pi\tilde{t}), \tag{B 22a,b}$$

https://doi.org/10.1017/jfm.2016.507 Published online by Cambridge University Press

the bulk solutions follow as

$$\hat{p}(k,\tilde{y},\tilde{t}) = \mathrm{i}\pi k\,\delta(|k|-2\pi)\exp\left(-\tfrac{1}{2}|k|\tilde{t}\right)\exp(-|k|\tilde{y}), \tag{B 23a}$$

$$\tilde{p}(\tilde{x},\tilde{y},\tilde{t}) = -2\pi\sin(2\pi\tilde{x})\exp(-2\pi\tilde{y})\exp(-\pi\tilde{t}), \tag{B 23b}$$

$$\hat{u}(k,\tilde{y},\tilde{t}) = -\frac{\mathrm{i}\hat{p}_0}{2k}(|k|\tilde{y}-1)\exp(-|k|\tilde{y}), \tag{B 23c}$$

$$\tilde{u}(\tilde{x},\tilde{y},\tilde{t}) = -\tfrac{1}{2}\cos(2\pi\tilde{x})(1-2\pi\tilde{y})\exp(-2\pi\tilde{y})\exp(-\pi\tilde{t}), \tag{B 23d}$$

$$\hat{v}(k,\tilde{y},\tilde{t}) = \tfrac{1}{2}\hat{p}_0\tilde{y}\exp(-|k|\tilde{y}), \tag{B 23e}$$

$$\tilde{v}(\tilde{x},\tilde{y},\tilde{t}) = -\tfrac{1}{2}\sin(2\pi\tilde{x})(2\pi\tilde{y})\exp(-2\pi\tilde{y})\exp(-\pi\tilde{t}), \tag{B 23f}$$

and the surfactant concentration is

$$\tilde{\Gamma}(\tilde{x}) = \sin(2\pi\tilde{x})\exp(-\pi\tilde{t}). \tag{B 24}$$

For the transient flow under a steady surfactant distribution, the surfactant distribution is

$$\tilde{\Gamma}(\tilde{x},\tilde{t}) = \sin(2\pi\tilde{x})\,H(\tilde{t}), \tag{B 25a}$$

$$\hat{\Gamma}(k,\tilde{t}) = -\mathrm{i}\pi\,\mathrm{sgn}(k)\,\delta(|k|-2\pi)\,H(\tilde{t}), \tag{B 25b}$$

$$\breve{\Gamma}(k,s) = -\frac{\mathrm{i}\pi}{s}\,\mathrm{sgn}(k)\,\delta(|k|-2\pi). \tag{B 25c}$$

Using (B 15), it follows that

$$\breve{p}_0(k,s) = \frac{\mathrm{i}k\pi}{s}\delta(|k|-2\pi), \tag{B 26}$$

and substitution into (B 12) provides:

$$\breve{u}_s(k,s) = -\frac{4\pi^3}{Re\,s^2}\delta(|k|-2\pi)\left[\sqrt{1+\frac{Re\,s}{4\pi^2}}-1\right], \tag{B 27a}$$

$$\hat{u}_s(k,\tilde{t}) = -\pi\delta(|k|-2\pi)\left[\frac{1}{2}\,\mathrm{erf}\left(\sqrt{t'}\right)-t'\,\mathrm{erfc}\left(\sqrt{t'}\right)+\sqrt{\frac{t'}{\pi}}\exp(-t')\right], \tag{B 27b}$$

$$\tilde{u}_s(\tilde{x},\tilde{t}) = -\cos(2\pi\tilde{x})\left[\frac{1}{2}\,\mathrm{erf}\left(\sqrt{t'}\right)-t'\,\mathrm{erfc}\left(\sqrt{t'}\right)+\sqrt{\frac{t'}{\pi}}\exp(-t')\right], \tag{B 27c}$$

where $t' = 4\pi^2\tilde{t}/Re$.

REFERENCES

BUSH, J. W. M. & HU, D. L. 2006 Walking on water: Biolocomotion at the interface. *Annu. Rev. Fluid Mech.* **38**, 339–369.

DLMF 2015 NIST Digital Library of Mathematical Functions http://dlmf.nist.gov/, Release 1.0.10 of 2015-08-07, online companion to Olver *et al.* (2010).

DUSSAUD, A. D. & TROIAN, S. M. 1998 Dynamics of spontaneous spreading with evaporation on a deep fluid layer. *Phys. Fluids* **10**, 23–38.

EDMONSTONE, B. D., CRASTER, R. V. & MATAR, O. K. 2006 Surfactant-induced fingering phenomena beyond the critical micelle concentration. *J. Fluid Mech.* **564**, 105–138.

https://doi.org/10.1017/jfm.2016.507 Published online by Cambridge University Press

ERDÉLYI, A., MAGNUS, W., OBERHETTINGER, F. & TRICOMI, F. G. 1954 *Tables of Integral Transforms*. McGraw-Hill.

FERNANDEZ, J. M. & HOMSY, G. M. 2004 Chemical reaction-driven tip-streaming phenomena in a pendant drop. *Phys. Fluids* **16**, 2548–2555.

GROTBERG, J. B. 1994 Pulmonary flow and transport phenomena. *Annu. Rev. Fluid Mech.* **26**, 529–571.

JENSEN, O. E. 1994 Self-similar, surfactant-driven flows. *Phys. Fluids* **6**, 1084–1094.

JENSEN, O. E. 1995 The spreading of insoluble surfactant at the free surface of a deep fluid layer. *J. Fluid Mech.* **293**, 349–378.

JENSEN, O. E. & GROTBERG, J. B. 1992 Insoluble surfactant spreading on a thin viscous film: shock evolution and film rupture. *J. Fluid Mech.* **240**, 259–288.

JENSEN, O. E. & NAIRE, S. 2006 The spreading and stability of a surfactant-laden drop on a prewetted substrate. *J. Fluid Mech.* **554**, 5–24.

KOHIRA, M. I., HAYASHIMA, Y., NAGAYAMA, M. & NAKATA, S. 2001 Synchronized self-motion of two camphor boats. *Langmuir* **17**, 7124–7129.

KOVALCHUK, V. I., KAMUSEWITZ, H., VOLLHARDT, D. & KOVALCHUK, N. M. 1999 Auto-oscillation of surface tension. *Phys. Rev.* E **60**, 2029–2036.

LAUGA, E. & DAVIS, A. M. J. 2012 Viscous Marangoni propulsion. *J. Fluid Mech.* **705**, 120–133.

LAVRENTEVA, O. M. & NIR, A. 2001 Spontaneous thermocapillary interaction of drops: unsteady convective effects at high Peclet numbers. *Phys. Fluids* **13**, 368–381.

LUCASSEN, J. 1968*a* Longitudinal capillary waves. Part 1: theory. *Trans. Faraday Soc.* **64**, 2221–2229.

LUCASSEN, J. 1968*b* Longitudinal capillary waves. Part 2: experiments. *Trans. Faraday Soc.* **64**, 2230–2235.

MASOUD, H. & SHELLEY, M. J. 2014 Collective surfing of chemically active particles. *Phys. Rev. Lett.* **112**, 128304.

MASOUD, H. & STONE, H. A. 2014 A reciprocal theorem for Marangoni propulsion. *J. Fluid Mech.* **741**, R4.

MATAR, O. K. & TROIAN, S. M. 1999 Spreading of a surfactant monolayer on a thin liquid film: onset and evolution of digitated structures. *Chaos* **9**, 141–153.

NAKATA, S., DOI, Y. & KITAHATA, H. 2005 Synchronized sailing of two camphor boats in polygonal chambers. *J. Phys. Chem.* B **109**, 1798–1802.

NAKATA, S. & HAYASHIMA, Y. 1998 Spontaneous dancing of a camphor scraping. *J. Chem. Soc. Faraday Trans.* **94**, 3655–3658.

NAKATA, S., IGUCHI, Y., OSE, S., KUBOYAMA, M., ISHII, T. & YOSHIKAWA, K. 1997 Self-rotation of a camphor scraping on water: new insight into the old problem. *Langmuir* **13**, 4454–4458.

OLVER, F. W. J., LOZIER, D. W., BOISVERT, R. F. & CLARK, C. W. (Eds) 2010 *NIST Handbook of Mathematical Functions*, Cambridge University Press; print companion to (DLMF 2015).

PIMIENTA, V. & ANTOINE, C. 2014 Self-propulsion on liquid surfaces. *Curr. Opin. Colloid Interface Sci.* **19**, 290–299.

RAYLEIGH, LORD 1890 Measurements of the amount of oil necessary in order to check the motions of camphor upon water. *Proc. R. Soc. Lond.* **47**, 364–367.

SCRIVEN, L. E. & STERNLING, C. V. 1960 The Marangoni effects. *Nature* **187**, 186–188.

STERNLING, C. V. & SCRIVEN, L. E. 1959 Interfacial turbulence: hydrodynamic instability and the Marangoni effect. *AIChE J.* **5**, 514–523.

STOCKER, R. & BUSH, J. W. M. 2007 Spontaneous oscillations of a sessile lens. *J. Fluid Mech.* **583**, 465–475.

THESS, A. 1996 Stokes flow at infinite Marangoni number: exact solutions for the spreading and collapse of a surfactant. *Phys. Scr.* T **67**, 96–100.

THOM, A. 1933 The flow past circular cylinders at low speeds. *Proc. R. Soc. Lond.* A **141**, 651–669.

TROIAN, S. M., HERBOLZHEIMER, E. & SAFRAN, S. A. 1990 Model for the fingering instability of spreading surfactant drops. *Phys. Rev. Lett.* **65**, 333–336.

VELARDE, M. G. & CHU, X.-L. 1989 Dissipative hydrodynamic oscillators. I: Marangoni effect and sustained longitudinal waves at the interface of two liquids. *Nuovo Cimento* D **11**, 709–716.

https://doi.org/10.1017/jfm.2016.507 Published online by Cambridge University Press